2017-10

Dynamic instability of laterally-restrained zed-purlin beams under uplift loading

Zhu, J

10.1016/j.ijmecsci.2017.07.021
International Journal of Mechanical Sciences
Elsevier BV

International Journal of Mechanical Sciences
http://dx.doi.org/10.1016/j.ijmecsci.2017.07.021
Accepted 9 July 2017

Dynamic instability of laterally-restrained zed-purlin beams under uplift loading

Jue Zhu[a], Shanguang Qian[b,c], Long-yuan Li[c]

(a) Faculty of Mechanical Engineering and Mechanics, Ningbo University, Ningbo 315211, PR China
(b) Faculty of Architechural Engineering, Kunming Metallurgy College, Kunming 650033, PR China (corresponding author, 308327174@qq.com, shanguang.qian@plymouth.ac.uk)
(c) School of Engineering, University of Plymouth, Plymouth PL4 8AA, UK

Abstract - This paper presents an analytical investigation on the free vibration, static buckling and dynamic instability of laterally-restrained zed-section purlin beams when subjected to uplift wind loading. The analysis is carried out by using the classical principle of minimum potential energy. By assuming the instability modes, the kinetic energy and strain energy of the beam and the loss of the potential energy of the applied load are evaluated, from which the mass, stiffness and geometric stiffness matrices of the system are derived. These matrices are then used to carry out the analyses of free vibration, static buckling and dynamic instability of the beams. Theoretical formulae are derived for the free vibration frequency, critical buckling moment, and excitation frequency of the beam. The effects of the section size of the beam and the static part of the applied load on the change of dynamic instability zone are also discussed.

Keywords: Cold-formed steel, buckling, dynamic instability, vibration, lateral-torsional, beam.

1. Introduction

Cold-formed steel (CFS) has been widely used in buildings to support roof and wall sheeting for the enclosure of the buildings. The benefits of using CFS sections are not only its high strength-to-weight ratio but also its lightness that can save costs on transport, erection and the construction of foundation, and flexibility that the members can be produced in a wide variety of sectional profiles, which can result in most cost effective designs. However, because of the feature of their open, thin, cross-sectional geometry, which gives great flexural rigidity about one axis at the expense of low flexural rigidity about a perpendicular axis and low torsional rigidity, the CFS structural members are susceptive to local, distortional, and lateral-torsional buckling [1], which can significantly affect the design strength of the members.

Literature survey on CFS sections shows a large resource of information that has been generated since the early work dating back to 1970's. The work involves the analysis of local, distortional, and lateral-torsional buckling of CFS columns and beams using analytical, numerical and experimental methods and the determination of design strengths of CFS structural members using effective width method and/or direct strength method. The details of the research development in the field can be found in the books specifically for CFS structures [2-7] and the

review articles on the research achievement of CFS sections [8-15]. New design specifications for CFS sections are also developed in recent years in Europe [16], North America [17] and Australia [18]. These specifications provide the basic rules and procedures to be followed in the design analysis of CFS sections and cover a number of aspects of CFS design. Despite this, however, there is one area where there is little research on CFS sections, which is the dynamic instability of CFS structural members when the applied load varies with time.

It is well-recognized that the dynamic characteristics of structures are very important. When design a structure in an earthquake zone, for example, one has to know the dynamic characteristics of the structure in order to avoid resonance disasters caused by the earthquake. It is known that the vibration in a structural member can reduce the critical load of buckling of the member. Hence, it is also important to study the dynamic load-induced instability of structures. The early work on the dynamic instability of elastic bodies was reported by Hsu in 1966 [19], who investigated the dynamic stability of the elastic body with given initial conditions and presented the necessary and sufficient stability criterions in terms of trajectories in the phase space of finite dimension. Huang and Hung studied the dynamic instability of a simply supported beam under periodic axial excitation by using the averaging method and the Routh-Hurwitz stability criteria [20]. The instability regions and vibration amplitudes was examined by considering the coupling of the first two modes. Park presented a finite element dynamic instability model of Timoshenko beams [21], in which the beam transverse motion in the plane was formulated through the extended Hamilton's principle. The dynamic instability of the beam was investigated by examining the divergence and flutter instabilities. The analysis showed that the effects of the rotary inertia and shear deformation parameters on the stable transverse motion of the beam are significant in certain ranges. More work on the dynamic instability of beams can be found in references [22-25]. The general theory of dynamic stability of elastic systems can be found in the book presented by Bolotin [26]. The use of finite element method for the analysis of dynamic stability of plates was first presented by Hutt and Salam [27]. The analysis of dynamic instability of structures using numerical methods are also available in references [28-30].

In this paper an analytical approach is proposed to analyze the dynamic instability of laterally-restrained zed-section beams under the action of an uplift wind load. The analysis is carried out by using the classical principle of minimum potential energy. By assuming the instability modes, the kinetic energy and strain energy of the beam and the loss of the potential energy of the applied load are evaluated, from which the mass, stiffness and geometric stiffness matrices of the system are derived. These matrices are then used to carry out the analyses of free vibration, static buckling and dynamic instability of the beams. Theoretical formulae are derived for the free vibration frequency, critical buckling moment, and excitation frequency of the beam.

2. Governing equation for dynamic instability analysis

The governing equation for the dynamic instability analysis of a structure can be expressed as follows [28-30],

$$[\mathbf{M}]\{\ddot{\mathbf{q}}\}+[\mathbf{K}]\{\mathbf{q}\}-\lambda[\mathbf{K}_g]\{\mathbf{q}\}=\{\mathbf{0}\} \tag{1}$$

where $[\mathbf{M}]$ is the mass matrix, $[\mathbf{K}]$ is the stiffness matrix, $[\mathbf{K}_g]$ is the geometric stiffness matrix, $\{\ddot{\mathbf{q}}\}$ is the generalized acceleration vector, $\{\mathbf{q}\}$ is the generalized displacement vector, and

λ is the loading factor. Assume that the externally applied load is periodic, in which case the loading factor can be divided into two parts as expressed in Eq.(2),

$$\lambda = \lambda_s + \lambda_t \cos \Omega t \tag{2}$$

where λ_s and λ_t are the amplitudes of the static and dynamic parts, respectively, Ω is the excitation frequency of the dynamic part of the load, and t is the time.

The dynamic instability regions of the structure described by Eq.(1) can be determined by periodic solutions with the periods of $T=2\pi/\Omega$ and $2T=4\pi/\Omega$ [28-30]. The solution with the period of $2T$ is of particular importance, representing the primary instability region of the structure, which can be expressed using the form of trigonometric series given by Eq.(3),

$$\{\mathbf{q}\} = \sum_{k=1,3,\cdots} \left[\{\mathbf{a}_k\} \sin \frac{k\Omega t}{2} + \{\mathbf{b}_k\} \cos \frac{k\Omega t}{2} \right] \tag{3}$$

where $\{\mathbf{a}_k\}$ and $\{\mathbf{b}_k\}$ are the vectors of coefficients of the assumed solution. Substituting Eqs.(2) and (3) into (1) and letting the coefficients of the series associated with $\sin(\Omega t/2)$ and $\cos(\Omega t/2)$ be zero, it yields,

$$\left([\mathbf{K}] - \frac{2\lambda_s - \lambda_t}{2} [\mathbf{K_g}] - \frac{\Omega^2}{4} [\mathbf{M}] \right) \{\mathbf{a}_1\} = \{\mathbf{0}\} \tag{4}$$

$$\left([\mathbf{K}] - \frac{2\lambda_s + \lambda_t}{2} [\mathbf{K_g}] - \frac{\Omega^2}{4} [\mathbf{M}] \right) \{\mathbf{b}_1\} = \{\mathbf{0}\} \tag{5}$$

For given values of λ_s and λ_t, one can calculate the two frequencies of Ω from Eqs.(4) and (5), which represent the boundary of dynamic instability regions of the structure analyzed.

Eqs.(4) and (5) are now applied to analyze the dynamic instability of a purlin-sheeting system under the action of a wind uplift load, as shown in Fig.1. In the system the uplift load acts on the sheeting, which is transferred to the purlin through the fixings and contact between the sheeting and upper flange of the zed-section purlin. The sheeting in the system provides translational and rotational restraints to the purlin due to its membrane and bending rigidities. For most types of sheeting the lateral displacement at the fixing point may be assumed to be completely restrained since the membrane rigidity of the sheet is sufficiently strong. However, the rotational restraint depends upon several factors, which contain the number, type and positions of the screws used for the fixings as well as the dimensions of purlin and sheeting. In the present study, the rotational restraint is ignored due to the weak bending rigidity of the sheeting and thus the corresponding results are considered to be conservative.

Let x, y, and z be the three coordinate axes of the right-hand rectangular coordinate system, with x being the longitudinal axis, y and z being the cross-sectional axes parallel to the web and flange lines, respectively. The origin of the coordinates is defined at the centroid of the section. Note that, for a zed-section of equal flanges the centroid and the shear centre are at the same point. Let v and w be the transverse and lateral displacement components of the beam at the centroid, and ϕ be the rotation of the beam section (see Fig.1). Since the lateral restraint provided by the sheeting is applied on the upper flange, w and ϕ must satisfy the following restraint condition [31,32],

$$w + \frac{h\phi}{2} = 0 \tag{6}$$

where h is the web depth. The kinetic energy and strain energy of the zed-section beam with simply supported boundary conditions due to the transverse displacement, lateral displacement and rotation thus can be expressed as

$$T = \frac{\rho A}{2}\int_o^l \left(\dot{v}^2 + \dot{w}^2\right)dx + \frac{\rho I_p}{2}\int_o^l \dot{\phi}^2 dx \tag{7}$$

$$U = \frac{1}{2}\int_o^l \left[EI_y(w'')^2 + 2EI_{yz}v''w'' + EI_z(v'')^2 + GJ(\phi')^2 + EI_w(\phi'')^2\right]dx \tag{8}$$

where ρ is the density, A is the cross-section area, I_p is the polar moment of inertia, E is the Young's modulus, G is the shear modulus, I_y and I_z are the second moments of area about y- and z-axis, I_{yz} is the product moment of area, J is the torsion constant, I_w is the warping constant, and l is the beam length. Note that the dot above a symbol in Eq.(7) represents the derivative of the symbol with respect to time t and the prime of a symbol in Eq.(8) represents the derivative of the symbol with respect to space coordinate x. Assume that the uplift load is applied on the upper flange along the web line of the zed-section beam. The loss of potential energy of the transverse load q_y can be expressed as [33,34],

$$V = \int_o^l M_z \phi w'' dx - \frac{a_y}{2}\int_o^l q_y \phi^2 dx \tag{9}$$

where q_y is the uplift distribution load, $M_z=q_y x(l-x)/2$ is the internal bending moment, and $a_y=h/2$ is the distance between the loading point and shear centre. Note that the pre-buckling bending about the minor axis for a zed-section beam can be normally ignored because of the restraint provided by the sheeting and thus the pre-buckling moment about minor axis is not included in Eq.(9). Assume that the transverse displacement v, lateral displacement w, and rotation ϕ of the beam can be expressed as follows,

$$v(x) = C_1(t)\sin\frac{\pi x}{l} \tag{10}$$

$$w(x) = C_2(t)\sin\frac{\pi x}{l} \tag{11}$$

$$\phi(x) = -\frac{2w(x)}{h} = -\frac{2C_2(t)}{h}\sin\frac{\pi x}{l} \tag{12}$$

where $C_j(t)$ (j=1,2) are the functions of time. Note that the displacement functions assumed here in Eqs.(10)-(12) satisfy all boundary conditions required for a simply support beam. The mass matrix of the zed-section beam can be obtained by substituting Eqs.(10)-(12) into (7), that is,

$$[\mathbf{M}] = \begin{bmatrix} \dfrac{\partial^2 T}{\partial \dot{C}_1^2} & \dfrac{\partial^2 T}{\partial \dot{C}_1 \partial \dot{C}_2} \\ \dfrac{\partial^2 T}{\partial \dot{C}_2 \partial \dot{C}_1} & \dfrac{\partial^2 T}{\partial \dot{C}_2^2} \end{bmatrix} = \begin{bmatrix} m_{11} & 0 \\ 0 & m_{22} \end{bmatrix} \tag{13}$$

in which, $m_{11} = \dfrac{\rho A l}{2}$ and $m_{22} = \dfrac{\rho A l}{2} + \dfrac{2\rho I_p l}{h^2}$.

The stiffness matrix of the zed-section beam can be obtained by substituting Eqs.(10)-(12) into (8), that is,

$$[\mathbf{K}]=\begin{bmatrix} \dfrac{\partial^2 U}{\partial C_1^2} & \dfrac{\partial^2 U}{\partial C_1 \partial C_2} \\ \dfrac{\partial^2 U}{\partial C_2 \partial C_1} & \dfrac{\partial^2 U}{\partial C_2^2} \end{bmatrix}=\begin{bmatrix} k_{11} & k_{12} \\ k_{21} & k_{22} \end{bmatrix} \tag{14}$$

in which, $k_{11}=\dfrac{EI_z l}{2}\left(\dfrac{\pi}{l}\right)^4$, $k_{12}=k_{21}=\dfrac{EI_{yz} l}{2}\left(\dfrac{\pi}{l}\right)^4$ and $k_{22}=\dfrac{EI_y l}{2}\left(\dfrac{\pi}{l}\right)^4\left(1+\dfrac{4I_w}{I_y h^2}+\dfrac{GJ}{EI_y}\left(\dfrac{2l}{\pi h}\right)^2\right)$.

The geometric stiffness matrix of the zed-section beam can be obtained by substituting Eqs.(10)-(12) into (9), that is,

$$[\mathbf{K}_g]=\begin{bmatrix} \dfrac{\partial^2 V}{\partial C_1^2} & \dfrac{\partial^2 V}{\partial C_1 \partial C_2} \\ \dfrac{\partial^2 V}{\partial C_2 \partial C_1} & \dfrac{\partial^2 V}{\partial C_2^2} \end{bmatrix}=\begin{bmatrix} 0 & 0 \\ 0 & k_{g22} \end{bmatrix} \tag{15}$$

in which, $k_{g22}=\dfrac{4M_o}{hl}\left(1+\dfrac{\pi^2}{3}-\dfrac{4a_y}{h}\right)$, where M_o= $q_y l^2/8$ is the largest pre-buckling moment in the beam span.

3. Free vibration

The free vibration frequencies of the laterally restrained zed-section beam can be calculated using Eq.(16)

$$\left\|[\mathbf{K}]-\omega^2[\mathbf{M}]\right\|=0 \tag{16}$$

where ω is the frequency. Substituting Eqs.(13) and (14) into (16), it yields,

$$\begin{aligned} \omega^2 &= \frac{(m_{11}k_{22}+m_{22}k_{11})\pm\sqrt{(m_{11}k_{22}+m_{22}k_{11})^2-4m_{11}m_{22}(k_{11}k_{22}-k_{12}^2)}}{2m_{11}m_{22}} \\ &= \frac{(m_{11}k_{22}+m_{22}k_{11})\pm\sqrt{(m_{11}k_{22}-m_{22}k_{11})^2+4m_{11}m_{22}k_{12}^2}}{2m_{11}m_{22}} \end{aligned} \tag{17}$$

The two frequencies given by Eq.(17) represent the translational and rotational vibrations of the laterally restrained zed-section beam. Fig.2 plots the variation of the two frequencies with the beam length for three typical section dimensions defined in Table 1, which are currently used in practice in UK market and represent small, medium and large size sections, respectively.

It can be seen from the figure that, for each section the frequencies of both the 1st and 2nd vibration modes decrease with the beam length, but the rate of decrease turns to be small with increased beam length. Also, it can be observed that, the larger the section size, the greater the frequencies. The comparison of the frequencies between the two vibration modes plotted in

Fig.3a and Fig.3b indicates that, the larger the section, the bigger the gap between the two frequencies. For example, the frequency of the 1st mode of the small, medium and large size beams of 7 m length is about 24, 28 and 41 rad/sec, respectively; whereas the frequency of the 2nd mode of these beams is about 53, 92, and 142 rad/sec, respectively. Note that because of the point-symmetry of the cross section and the lateral restraint applied at the upper flange the transverse and lateral vibration modes and the rotational vibration mode are all coupled each other. In other words, the 1st vibration mode represents neither the translational vibration mode nor the rotational vibration mode, but a combination of the two modes.

4. Buckling analysis

The buckling of the laterally restrained zed-section beam subjected to static load can be analyzed as follows,

$$\left\| [\mathbf{K}] - \lambda_{cr} [\mathbf{K}_g] \right\| = 0 \tag{18}$$

where λ_{cr} is the loading factor and $M_{cr}=\lambda_{cr}M_o$ is the critical moment for static buckling. Substituting Eqs.(14) and (15) into (18), it yields,

$$\lambda_{cr} = \frac{k_{11}k_{22} - k_{12}^2}{k_{11}k_{g22}} = \left(\frac{\pi^2 h}{4l}\right)^2 \left(\frac{2EI_z}{M_o h}\right) \frac{\dfrac{I_y}{I_z} + \dfrac{4I_w}{I_z h^2} + \dfrac{GJ}{EI_z}\left(\dfrac{2l}{\pi h}\right)^2 - \left(\dfrac{I_{yz}}{I_z}\right)^2}{1 + \dfrac{\pi^2}{3} - \dfrac{4a_y}{h}} \tag{19}$$

The critical moments of the small, medium and large size beams calculated using Eq.(19) are plotted in Fig.3, in which Figs.3a and 3b are for the uplift loads that are applied at the upper flange ($a_y=h/2$) and at the shear centre ($a_y=0$), respectively. In order to demonstrate the appropriateness of the present model the critical moments computed from the semi-analytical finite strip analysis [35,36] are also plotted in Fig.3b, in which the trigonometric series describing the variation of displacement functions along the x-axis are all coupled and thus enable the effect of pre-buckling moment gradient to be taken into account. It is evident from the figure that the critical moments calculated from the present simple model are very close to those computed using the semi-analytical finite strip analysis method.

As is to be expected, for each section the critical moment decreases with the increase of beam length. The larger the section size, the higher the critical moment. Also, it can be found from the comparison of the buckling curves shown in Fig.3a and 3b that, the position where the load is applied has a significant effect on the critical moment. For example, when the load is applied at the shear centre the critical moment of the small, medium and large size beams of 7 m length is about $0.102M_y$, $0.125M_y$ and $0.262M_y$, respectively; whereas the load is applied at the upper flange the critical moment of these beams is about $0.192M_y$, $0.235M_y$ and $0.490M_y$, respectively. The reason for this is similar to what is explained in the references [33,34].

5. Dynamic instability analysis

The dynamic instability regions of the laterally restrained zed-section beam can be calculated using Eq.(20), which can be derived from Eqs.(4) and (5),

$$\left\| [\mathbf{K}] - \frac{2\lambda_s \pm \lambda_t}{2}[\mathbf{K_g}] - \frac{\Omega^2}{4}[\mathbf{M}] \right\| = 0 \tag{20}$$

Substituting Eqs.(13), (14) and (15) into (20), it yields,

$$\frac{\Omega^2}{4} = \frac{(m_{11}k_{22}^* + m_{22}k_{11}) \pm \sqrt{(m_{11}k_{22}^* - m_{22}k_{11})^2 + 4m_{11}m_{22}k_{12}^2}}{2m_{11}m_{22}} \tag{21}$$

where $k_{22}^* = k_{22} - \left(\lambda_s \pm \frac{\lambda_t}{2}\right)k_{g22}$. Note that Eq.(21) represents four different equations from which four different Ω^2 values can be obtained. As is demonstrated in the free vibration analysis shown in Section 3, the frequency associated with the 2nd vibration mode is much greater than that associated with the 1st vibration mode. Hence, only the 1st vibration mode need be considered when calculating the dynamic instability regions. In this case, Eq.(21) can be simplified as follows,

$$\frac{\Omega^2}{4} = \frac{(m_{11}k_{22}^* + m_{22}k_{11}) - \sqrt{(m_{11}k_{22}^* - m_{22}k_{11})^2 + 4m_{11}m_{22}k_{12}^2}}{2m_{11}m_{22}} \tag{22}$$

For the simplicity of presentation, in the following dynamic instability analysis the reference moment M_o used in the calculation of geometric stiffness matrix is assumed to be $M_o=M_{cr}$. Thus, for a given value of λ_s (λ_s <1 because $\lambda_s M_o=\lambda_s M_{cr}$ must be less than M_{cr}) one can obtain two sets of values of Ω^2 for a given set of values of λ_t. These two sets of Ω^2 values form the dynamic instability region of the laterally restrained zed-section beam.

Fig.4 shows the dynamic instability region of the laterally-restrained zed-section beams of 7 m length, under an uplift periodic load applied at the upper flange of the beams. It can be seen from the figure that, the dynamic instability regions of the three beams all exhibit like a "v" shape although they have different widths. With the increase of section size of the beam the dynamic instability zone not only moves towards to higher frequency side but its width is also expanded.

Fig.5 shows the dynamic instability region of the laterally-restrained zed-section beams of 7 m length, under a combined static and periodic load applied at the upper flange of the beams. It can be seen from the figure that, when a static load of 20% of the critical load is involved, the dynamic instability zone shifts to lower frequency side and the corresponding width is largely extended. With the further increase in the value of the static load, the dynamic instability zone moves further towards to the lower frequency side and its width is continuously expanded as is demonstrated in Fig.6. Note that, in all cases, the variation of the dynamic instability zone due to either the section size change or the loading type change of the beam can be characterised by the "shift" of the right-side arm and the "shift" plus "twisting" of left-side arm of the instability zone.

6. Conclusions

This paper has presented an analytical investigation on the dynamic instability of laterally-restrained zed-section purlin beams under the action of uplift wind loading. By assuming the instability modes, the kinetic energy and strain energy of the beam and the loss of the potential energy of the applied load have been evaluated using the theory of classical elastic mechanics, from which the mass, stiffness and geometric stiffness matrices of the system are derived. These matrices are then used to carry out the analyses of free vibration, static buckling and dynamic instability of the beams. The following conclusions are drawn from the obtained results:

- There is a modal coupling between the translational and rotational modes in the free vibration, static buckling and dynamic instability analyses of the laterally-restrained zed-section purlin beams under the action of uplift wind loading.
- Both the frequency and critical buckling moment of the beam can be increased by increasing the beam section size. However, the effectiveness of doing so decreases with increased beam length.
- The increase of the section size of the zed-purlin leads to a shift of the dynamic instability zone towards to higher frequency side and the broad up of the width of the instability zone.
- When the applied load involves also a static load the dynamic instability zone will shift towards to lower frequency side and the width of the dynamic instability zone of the beam will be also expanded.

Acknowledgements - The authors acknowledge the financial support received from National Natural Science Foundation of China (No.11572162). The first author also wishes to acknowledge the 47th Scientific Research Foundation for Returned Scholars from Ministry of Education of China, Natural Science Foundation of Zhejiang Province (No.LY13A020007), and K.C. Wong Magna Fund at Ningbo University for their financial support. The second author wishes to acknowledge the China Scholar Council (CSC) for supporting him to visit the University of Plymouth.

References

[1] Hancock GJ. Local, distortional and lateral buckling of I-beams. Journal of Structural Division ASCE 1978; 104(11): 1787-1798.
[2] Walker AC. Design and Analysis of Cold-formed Sections, 1975, International Textbook Company Ltd, London.
[3] Rhodes J. Design of Cold-formed Steel Members, 1991, Elsevier Applied Science, London.
[4] Rhodes J, Lawson RM. Design of Structures Using Cold-formed Steel Sections (SCI Publication 089), 1992, The Steel Construction Institute, Ascot, UK.
[5] Yu WW. Cold-formed Steel Design, 2000, John Wiley and Sons, New-York.
[6] Hancock GJ, Murray TM, Ellifritt DS. Cold-formed Steel Structures to the AISI Specification, 2001, CRC Press, Taylor and Francis Group, New York.
[7] Hancock GJ. Design of Cold-formed Steel Structures to AS/NZS 4600:2005, 2008, Australia Steel Institute, Sydney, Australia.

[8] Hancock GJ. Light gauge construction. Prog. Struct. Engng. Mater. 1997; 1(1): 25-30.
[9] Davies JM. Recent research advances in cold-formed steel structures. Journal of Constructional Steel Research 2000; 55(1-3): 267–288.
[10] Rondal J. Cold formed steel members and structures – general report. Journal of Constructional Steel Research 2000; 55(1-3): 155–158.
[11] Hancock GJ. Cold-formed steel structures. Journal of Constructional Steel Research 2003; 59(4): 473–487.
[12] Macdonald M, Heiyantuduwa MA, Rhodes J. Recent developments in the design of cold-formed steel members and structures. Thin-Walled Structures 2008; 46(7-9): 1047-1053.
[13] Schafer BW. Review: the direct strength method of cold-formed steel member design. Journal of Constructional Steel Research 2008; 64(7/8): 766–778.
[14] Li LY. Calculation of moment capacity of cold-formed steel members. International Journal of Structural Engineering 2011; 2(2): 101-115.
[15] Hancock GJ. Cold-formed steel structures: Research review 2013–2014. Advances in Structural Engineering 2016; 19(3): 1–16.
[16] EN1993-1-3. Eurocode 3 - Design of Steel Structures - Part 1-3: General rules - Supplementary rules for cold-formed members and sheeting, 2006, BSI, London.
[17] AISI. Specification for the design of cold-formed steel structural members, Cold-formed Steel Design Manual – Part V, 2004, Washington DC.
[18] AS/NZS. Australian/New Zealand Standard on Cold-formed Steel Structures – AS/NZS-4600 (2nd ed.), 2005, Standards of Australian and Standards of New Zealand, Sydney-Wellington.
[19] Hsu CS. On dynamic stability of elastic bodies with prescribed initial conditions. International Journal of Engineering Science 1966; 4(1): 1-21.
[20] Huang JS, Hung LH. Dynamic stability for a simply supported beam under periodic axial excitation. International Journal of Non-Linear Mechanics 1984; 19(4): 287-301.
[21] Park YP. Dynamic stability of a free Timoshenko beam under a controlled follower force. Journal of Sound and Vibration 1987; 113(3): 407-415.
[22] Majorana CE, Pomaro B. Dynamic stability of an elastic beam with visco-elastic translational and rotational supports. Engineering Computations 2011; 28(2): 114–129.
[23] Majorana CE, Pomaro B. Dynamic stability of an elastic beam with visco-elasto-damaged translational and rotational supports. Journal of Engineering Mechanics (ASCE) 2012; 138(6): 582–590.
[24] Chang CS, Hodges DH. Stability studies for curved beams. Journal of Mechanics of Materials and Structures 2009; 4(7/8): 1257-1270.
[25] Challamel N, Casandjian C, Lerbet J. On the occurrence of flutter in the lateral-torsional instabilities of circular arches under follower loads. Journal of Sound and Vibration 2009; 320(3): 617-631.
[26] Bolotin VV. The Dynamic Stability of Elastic Systems, 1964, San Francisco, CA, Holden-day, Inc.
[27] Hutt JM, Salam AE. Dynamic stability of plates by finite element method. Journal of Engineering Mechanics (ASCE) 1971; 97(3): 897-899.
[28] Patel SN, Datta PK, Sheikh AH. Buckling and dynamic instability analysis of stiffened shell panels. Thin-Walled Structures 2006; 44(3): 321-333.
[29] Kratzig WB, Li LY, Nawrotzki P. Stability conditions for non-conservative dynamical systems. Computational Mechanics 1991; 8(3): 145-151.

[30] Li LY, Interaction of forced and parametric loading vibrations. Computers and Structures 1991; 40(3): 615-618.
[31] Li LY. Lateral-torsional buckling of cold-formed zed-purlins partial-laterally restrained by metal sheeting. Thin-Walled Structures 2004; 42(7): 995–1011.
[32] Ye ZM, Kettle R, Li LY. Analysis of cold-formed zed-purlins partially restrained by steel sheeting. Computer and Structures 2004; 82(9/10) 731–739.
[33] Yoo CH, Lee SC. Stability of structures, principles and applications. Butterworth-Heinemann, 2011, Kidlington, Oxford, UK.
[34] Timoshenko SP, Gere JM. Theory of Elastic Stability (2nd edition), McGraw-Hill Book Company, 1961, New York.
[35] Chu XT, Ye ZM, Kettle R, Li LY. Buckling behaviour of cold-formed channel sections under uniformly distributed loads. Thin-Walled Structures 2005; 43(4): 531-542.
[36] Chu XT, Ye ZM, Li LY, Kettle R. Local and distortional buckling of cold-formed zed-section beams under uniformly distributed transverse loads. International Journal of Mechanical Sciences 2006; 48(4): 378–388.

Table 1. Section dimensions of zed-section beams

Section	Web depth *h* (mm)	Flange width *b* (mm)	Lip length *c* (mm)	Thickness *t* (mm)
A	120	50	15	1.5
B	225	65	20	2.0
C	345	100	30	2.5

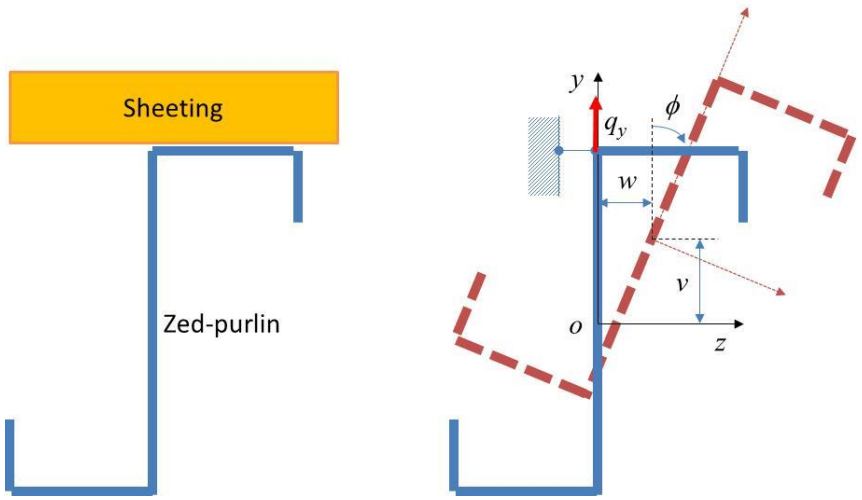

(a) (b)

Figure 1. (a) Sheeting-purlin system. (b) Definition of lateral-torsional displacements.

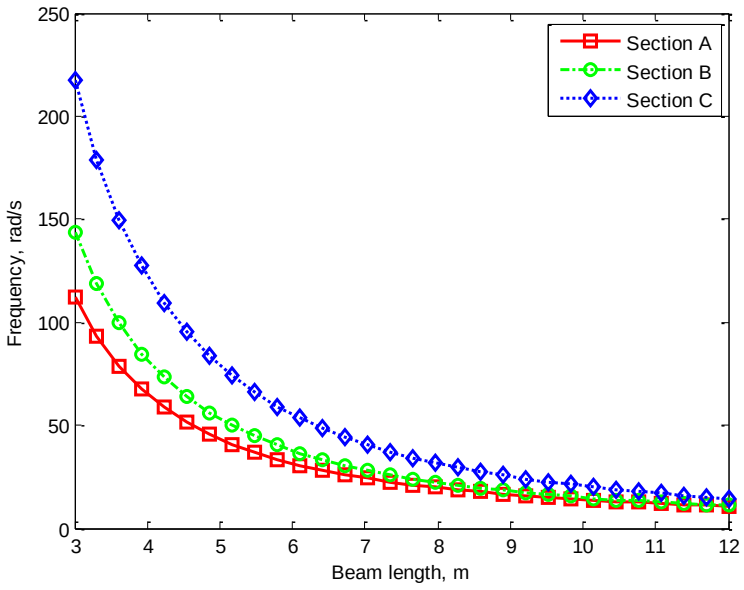

(a)

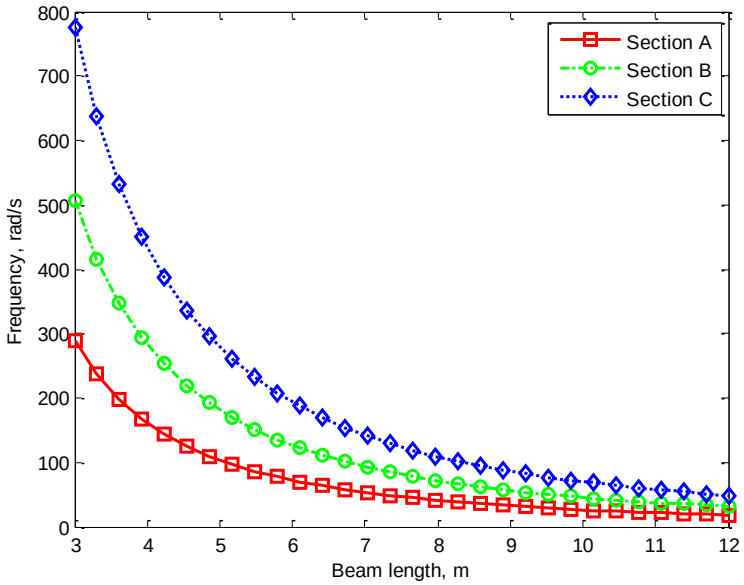

(b)

Figure 2. Frequency of laterally-restrained zed-section beams. (a) 1st mode and (b) 2nd mode.

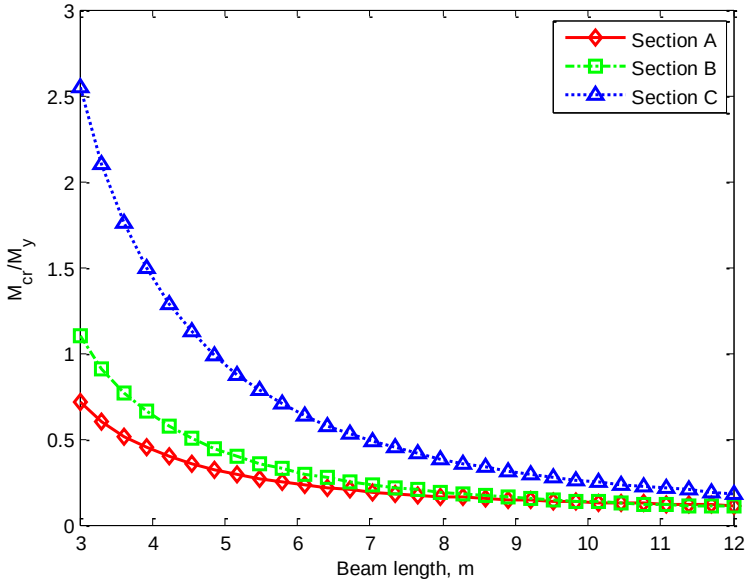

(a)

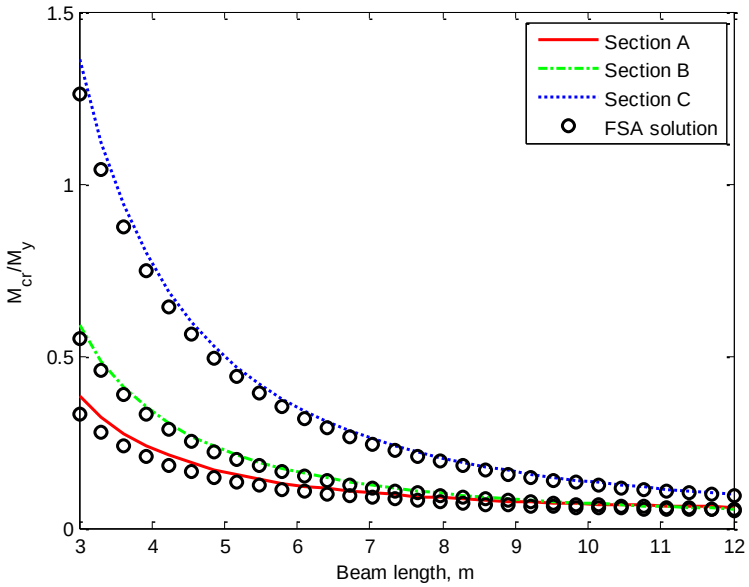

(b)

Figure 3. Critical moment of laterally-restrained zed-section beams ($M_y=2\sigma_y I_z/h$ is the yield moment). (a) Load acts at top flange and (b) load acts at shear centre.

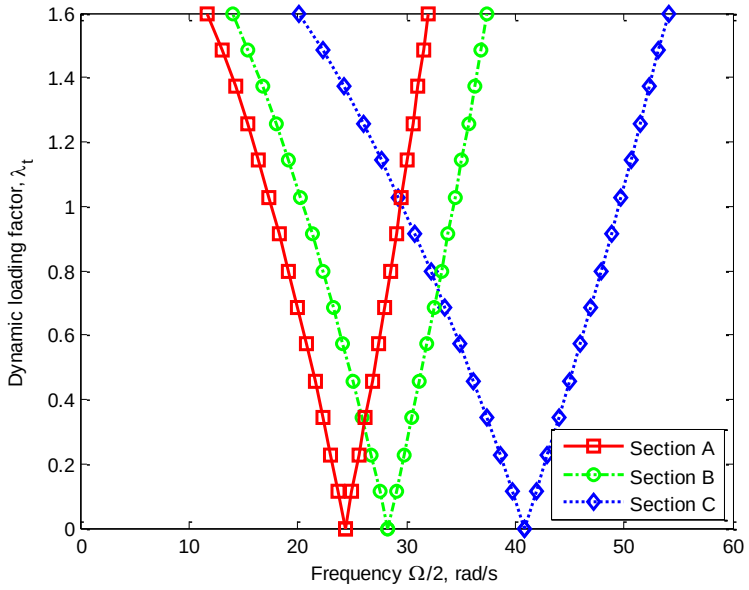

Figure 4. Dynamic instability region of laterally-restrained zed-section beams (λ_s=0, M_o=M_{cr}).

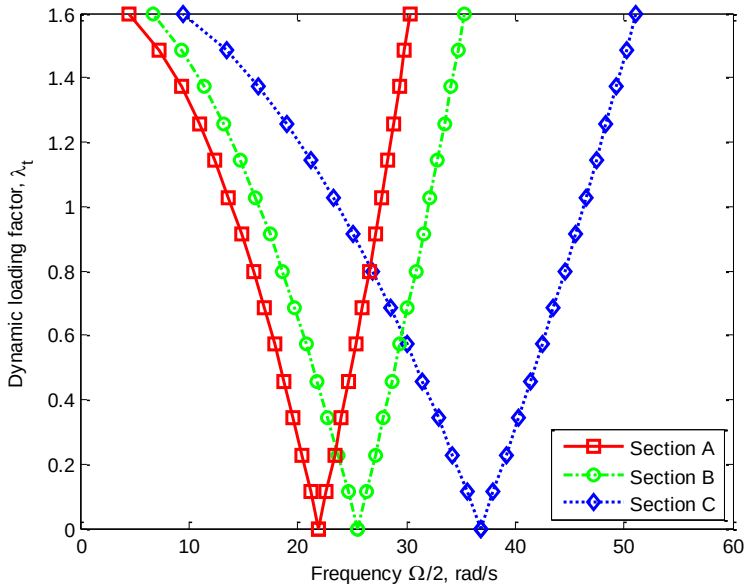

Figure 5. Dynamic instability region of laterally-restrained zed-section beams (λ_s=0.2, M_o=M_{cr}).

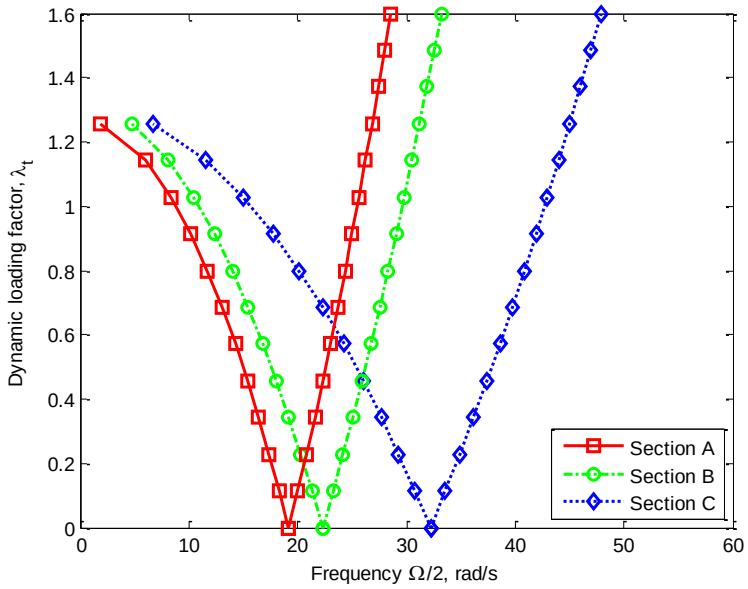

Figure 6. Dynamic instability region of laterally-restrained zed-section beams (λ_s=0.4, M_o=M_{cr}).